Title

Electrical and Optical Tunability in All-Inorganic Halide Perovskite Alloy Nanowires.

Journal

Nano letters, 18(6)

ISSN

1530-6984

Authors

Lei, Teng
Lai, Minliang
Kong, Qiao
et al.

Publication Date

2018-06-01

DOI

10.1021/acs.nanolett.8b00603

Peer reviewed

NANO LETTERS
Cite This: Nano Lett. 2018, 18, 3538−3542
Letter
pubs.acs.org/NanoLett

Electrical and Optical Tunability in All-Inorganic Halide Perovskite Alloy Nanowires

Teng Lei,[†] Minliang Lai,[†] Qiao Kong,[†] Dylan Lu,[†] Woochul Lee,[‡] Letian Dou,[§] Vincent Wu,[∥] Yi Yu,[⊥] and Peidong Yang*[,†,#,∇,○]

[†]Department of Chemistry, University of California, Berkeley, Berkeley, California 94720, United States
[‡]Department of Mechanical Engineering, University of Hawaii at Manoa, Honolulu, Hawaii 96822, United States
[§]Davidson School of Chemical Engineering, Purdue University, West Lafayette, Indiana 47907, United States
[∥]Department of Chemical & Biomolecular Engineering, University of California, Berkeley, Berkeley, California 94720, United States
[⊥]School of Physical Science and Technology, Shanghai Tech University, Shanghai 201210, China
[#]Materials Sciences Division, Lawrence Berkeley National Laboratory, Berkeley, California 94720, United States
[∇]Department of Materials Science and Engineering, University of California, Berkeley, Berkeley, California 94720, United States
[○]Kavli Energy NanoScience Institute, Berkeley, California 94720, United States

Supporting Information

ABSTRACT: Alloying different semiconductors is a powerful approach to tuning the optical and electronic properties of semiconductor materials. In halide perovskites (ABX_3), alloys with different anions have been widely studied, and great band gap tunability in the visible range has been achieved. However, perovskite alloys with different cations at the "B" site are less understood due to the synthetic challenges. Herein, we first have developed the synthesis of single-crystalline $CsPb_xSn_{1-x}I_3$ nanowires (NWs). The electronic band gaps of $CsPb_xSn_{1-x}I_3$ NWs can be tuned from 1.3 to 1.78 eV by varying the Pb/Sn ratio, which leads to the tunable photoluminescence (PL) in the near-infrared range. More importantly, we found that the electrical conductivity increases as more Sn^{2+} is alloyed with Pb^{2+}, possibly due to the increase of charge carrier concentration when more Sn^{2+} is introduced. The wide tunability of the optical and electronic properties makes $CsPb_xSn_{1-x}I_3$ alloy NWs promising candidates for future optoelectronic device applications.

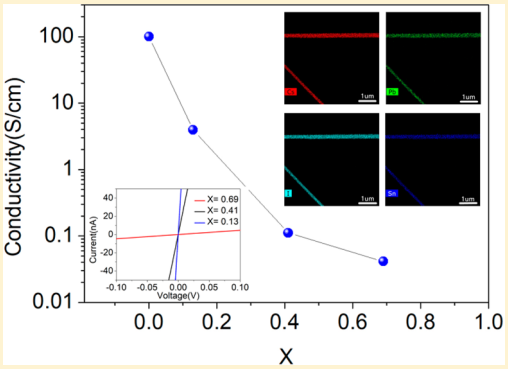

KEYWORDS: *Semiconductor alloy, tunability, halide perovskite, nanowires*

Semiconductor alloys have been widely used in numerous technologies, such as solar cells,[1−5] laser diodes,[5,6] and heterojunction bipolar transistors.[7] The band gap engineering of semiconductor alloys can be used to reach desired optical and electrical properties.[3,8,9] For instance, the graded-gap semiconductor alloy, such as $Cu(In_{1-x}Ga_x)Se_2$, has significantly improved the absorption of light and thus the power conversion efficiency (PCE) for photovoltaic application.[1,2] In addition, heterojunction bipolar transistors utilize alloy base layers to enhance the emitter injection efficiency, thus contributing to fast transistors.[10] Therefore, investigation of semiconductor alloys' structural, optical, and electrical properties is essential to pave the way for further application in optoelectronic devices.

Halide perovskites, an emerging class of semiconductor materials, have attracted much more attention in recent years due to their breakthrough performance as photovoltaic materials.[11−15] They have also been demonstrated as promising candidates for other optoelectronic applications, such as light-emitting diodes,[16] lasers,[17−19] and photodetectors.[20,21] In the push to further improve PCE of solar cells, it is essential to find an ideal light harvester with a band gap between 1.15 and 1.4 eV that can absorb all visible as well as some of the near-infrared light of the solar spectrum, thus reaching an ideal PCE according to the Shockley−Queisser limit. Alloying different semiconductors offers a good approach to tuning the band gap. By synthesizing tin−lead alloy perovskite materials, the band gap can be decreased to as low as 1.2 eV,[4] which paves the way toward high-efficiency perovskite−perovskite tandem photovoltaics. However, most of the previous studies about mixed cation perovskite alloy materials were based on polycrystalline perovskite films deposited on the substrates using deposition of a mixture of different AX and BX_2 (A = Cs, MA, or FA; B = Pb or Sn; X = Cl, Br, or I) solutions.[22] The uncontrolled

Received: February 11, 2018
Revised: April 14, 2018
Published: May 17, 2018

DOI: 10.1021/acs.nanolett.8b00603
Nano Lett. 2018, 18, 3538−3542

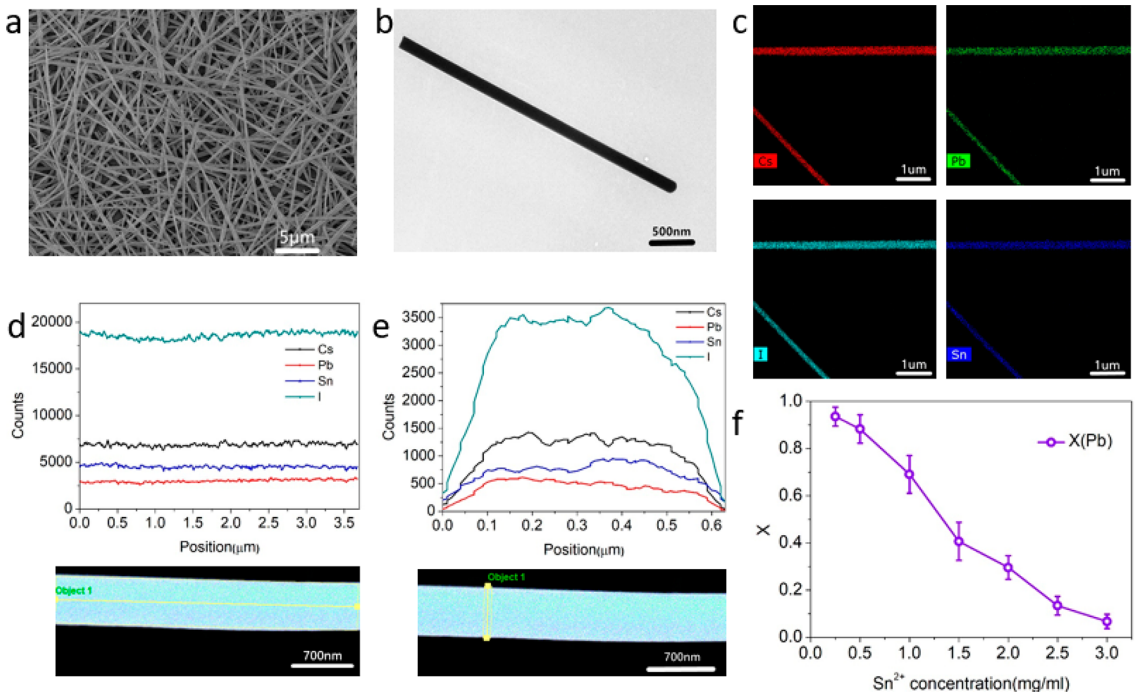

Figure 1. Synthesis and composition characterizations of as-synthesized yellow phase $CsPb_xSn_{1-x}I_3$ nanowires. (a) Scanning electron microscopy (SEM) image of $CsPb_xSn_{1-x}I_3$ (x = 0.30) nanowire mesh grown on glass substrate. (b) Transmission electron microscopy (TEM) image of a single $CsPb_xSn_{1-x}I_3$ (x = 0.30) nanowire. (c) EDS mapping of $CsPb_xSn_{1-x}I_3$ (x = 0.30) nanowires showing individual maps from the Cs L-edge, Pb L-edge, Sn L-edge, and I L-edge. (d, e) Line scan along and across the $CsPb_{1-x}Sn_xI_3$ (x = 0.30) nanowire, showing uniform elemental distribution. (f) Relation of the NWs' composition as the concentration of Sn precursor.

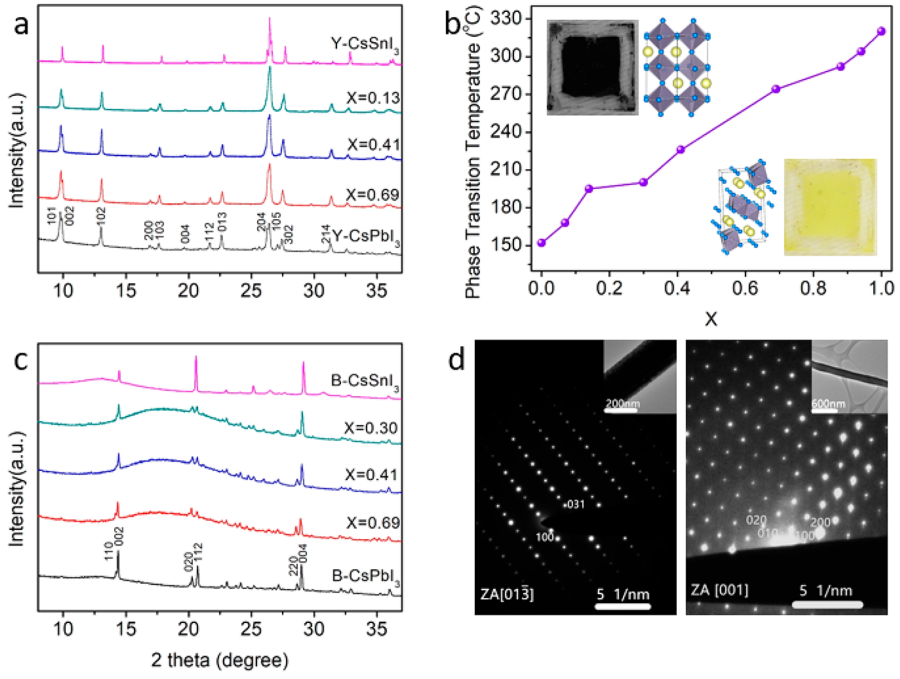

Figure 2. Structural characterization of both yellow and black phase $CsPb_xSn_{1-x}I_3$. (a) XRD patterns of as-synthesized yellow phase $CsPb_xSn_{1-x}I_3$ NWs as well as (c) converted black phase $CsPb_xSn_{1-x}I_3$ NWs. (b) Plots of phase transition temperature as a function of the Pb content. The images of yellow and black phase $CsPb_xSn_{1-x}I_3$ (x = 0.30) NW mesh and structures are inset. (d) SAED patterns of an individual yellow (left) and black (right) phase $CsPb_xSn_{1-x}I_3$ (x = 0.30) nanowire. TEM image of the same nanowire is shown in inset.

crystallization, precipitation, or evaporation produces morphological variations and grain boundaries that may hinder the understanding of the intrinsic properties for mixed cation alloy materials.

Among the halide perovskites, cesium lead iodide ($CsPbI_3$) features a suitable band gap (1.78 eV), nanoscale stability, and long charge carrier lifetime for photovoltaic application.[23] $CsSnI_3$ has also been used as an effective hole transport material to replace the unstable organic liquid electrolytes in

DOI: 10.1021/acs.nanolett.8b00603
Nano Lett. 2018, 18, 3538−3542

solid-state dye-sensitized solar cells, and can enhance visible light absorption in the near-infrared region with a band gap of 1.3 eV.[24−26] Although both the $CsPbI_3$ and $CsSnI_3$ have quite similar composition and crystal structure, their optical and electrical properties are quite different.[26,27] These interesting properties intrigue us to synthesize the $CsPb_xSn_{1-x}I_3$ nanowires (NWs) with precisely controlled physical properties for further nanoelectronics applications.

Here, we report the first synthesis of $CsPb_xSn_{1-x}I_3$ NWs and systematically study the composition and structure of these alloy nanomaterials, as well as their optical, electrical, and phase transition properties. Both $CsPbI_3$ and $CsSnI_3$ have four different polymorphs (yellow, black-α, black-β, and black-γ), among which yellow phase (Y) with a double chain structure is the thermodynamically stable phase at room temperature, and black orthorhombic phase (B-γ) with a distorted perovskite structure has been widely explored which shows excellent optical properties.[25,27] Similar to $CsPbI_3$ and $CsSnI_3$, Y and B-γ phases of $CsPb_xSn_{1-x}I_3$ show dramatic difference in both optical and electrical properties. Y phase $CsPb_xSn_{1-x}I_3$ NWs are indirect band gap semiconductors with weak photoluminescence, while B-γ phase $CsPb_xSn_{1-x}I_3$ NWs behave as direct band gap semiconductors with PL tunability in the near-IR range (λ = 700−950 nm). In addition, both Y and B-γ phases $CsPb_xSn_{1-x}I_3$ exhibit electrical conductivity tunability as the composition changes.

We developed a two-step method to synthesize the Y phase $CsPb_xSn_{1-x}I_3$ NWs at room temperature. Generally, PbI_2 thin film was made by spin coating the PbI_2 (in DMF) on a glass substrate, which was then immersed in a solution of CsI and SnI_2 for 12 h. A Y phase $CsPb_xSn_{1-x}I_3$ NW mesh was formed due to the anisotropic structure (Figure 1a). The transmission electron microscopy (TEM) image shows that the NW has well-defined morphology (Figure 1b). Generally, the diameter of the nanowires ranges from 100 to 500 nm, and the length is 5−50 μm from our SEM and TEM measurement. Energy-dispersive X-ray spectroscopy (EDS) mapping clearly shows the homogeneous distribution of Cs, Pb, Sn, and I in the NWs on the 100 nm scale (Figure 1c). To investigate the distribution of Pb and Sn in the NWs at a smaller scale, line scans along (Figure 1d) and across (Figure 1e) the NW were taken, which demonstrate the homogeneous distribution at the 10 nm scale. The line scan quantifications show the composition of the NW along the line (Figure S2). EDS quantification on different areas within a NW also further proved the homogeneous distribution of Pb and Sn (Figure S3). By varying the concentration of SnI_2 in the precursor solution, the composition of Pb (X), can be tuned from 0.07 to 0.94 (Figure 1f).

The crystal structure of $CsPb_xSn_{1-x}I_3$ NWs was studied by X-ray diffraction (XRD) and selected area electron diffraction (SAED). The XRD patterns of the as-synthesized Y phase $CsPb_xSn_{1-x}I_3$ NWs (Figure 2a) were assigned to the non-perovskite orthorhombic phase $CsPb_xSn_{1-x}I_3$, which is similar to the nonperovskite orthorhombic phase of $CsPbI_3$ with edge-shared PbI_6 octahedra in a double chain structure. No patterns from the starting materials PbI_2, SnI_2, or CsI were observed in XRD measurement. The lattice constants of Y phase $CsPbI_3$ and $CsSnI_3$ are quite close, which results in the similarity of XRD patterns. Therefore, the peak shifts caused by the lattice constant change as the composition varies are not obvious for Y phase $CsPb_xSn_{1-x}I_3$ NWs, but we can still observe the gradual shift in the (002), (013), and (105) peaks after inspecting the magnified patterns.

The Y and black phases of $CsPb_xSn_{1-x}I_3$ NWs can be interconverted. At room temperature, the as-synthesized $CsPb_xSn_{1-x}I_3$ NWs were Y phase, and temperature was increased to initiate the phase change to black phase. By heating the Y phase $CsPb_xSn_{1-x}I_3$ NWs up to the phase transition temperature in the glovebox and quenching them quickly to room temperature, B-γ phase $CsPb_xSn_{1-x}I_3$ NWs were obtained (Figure 2b inset). We found that the phase transition temperature is related to the specific composition of the NWs. The phase transition temperature increases as the Pb concentration increases in NWs, and it can be tuned from 152 to 320 °C (Figure 2b). The phase transition temperature for the x = 0.30 composition was confirmed by differential scanning calorimetry (DSC) (Figure S4). The peak at 200 °C corresponds to the yellow phase to black phase transition, which confirms our measurement from an infrared thermometer (199 °C).

Due to the air instability of the B-γ phase $CsPb_xSn_{1-x}I_3$ NWs, we coated the NWs with UV curing epoxy to protect them during the XRD measurement. The broad background results from the UV curing epoxy. From the XRD result of the black phase $CsPb_xSn_{1-x}I_3$ NWs (Figure 2c), it is clear that there are no peaks corresponding to the Y phase $CsPb_xSn_{1-x}I_3$ NWs, or the peaks from CsI, PbI_2, or SnI_2, which demonstrates the successful phase transition without the observable decomposition. Their XRD patterns can be assigned to the black orthorhombic perovskite (B-γ) phase, which is the tilted perovskite structure. The split peaks at about 14°, 20°, and 28° and the smaller peaks between 20° and 28° are the important indicators for this phase. The structures of both Y (Figure 2d left) and B-γ (Figure 2d right) phase $CsPb_xSn_{1-x}I_3$ NWs were further confirmed by SAED, which also indicates the single-crystalline NWs. More SAED patterns from different zone axes are shown in the Supporting Information (Figure S5). Representative high-resolution TEM images of as-grown $CsPb_xSn_{1-x}I_3$ NWs further indicate single-crystalline structure (Figure S6).

The Y phase $CsPb_xSn_{1-x}I_3$ NWs are indirect band gap semiconductors. The band gaps calculated from absorption spectra were fit to a binomial relation dependent on the composition of Pb (Figure S7a), showing a bowing effect with bowing parameters of 0.35 eV. Similar bowing is known for halide alloy perovskite,[28] as well as other semiconductor alloys, such as zinc chalcogenide or group-III nitride alloys.[29] Due to the sensitivity of Sn^{2+} in air condition, all the PL measurements were carried out in an argon-filled air-free cell. The PL spectrum of the Y phase $CsPbI_3$ NWs shows two broad emission peaks centered at about 450 and 530 nm which are attributed to excitonic emission and exciton self-trapping, respectively,[30] while the Y phase $CsSnI_3$ only reveals a broad emission peak at 700 nm, and no band edge emission was observed from our measurement. Interestingly, all Y phase $CsPb_xSn_{1-x}I_3$ NWs show broad emission around 700 nm, which may be attributed to exciton self-trapping similar to the broad emission from $CsPbI_3$ at around 530 nm (Figure S7b). It is likely that the incorporation of Sn leads to some trap states below the conduction band minimum, resulting in the emission at 700 nm. The B-γ phase $CsPb_xSn_{1-x}I_3$ NWs are direct band gap semiconductors. Calculated band gaps from Tauc plots (Figure S8) which are derived from the absorption spectrum (Figure S9) demonstrate the band gap tunability from 1.3 to

DOI: 10.1021/acs.nanolett.8b00603
Nano Lett. 2018, 18, 3538−3542

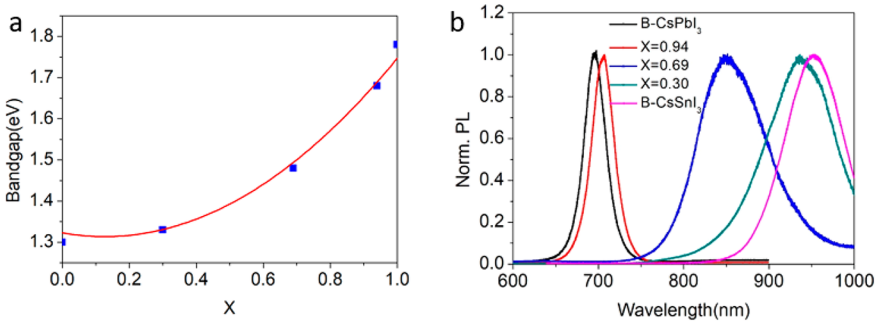

Figure 3. Optical properties of black phase $CsPb_xSn_{1-x}I_3$ nanowires. (a) Calculated band gaps of black phase $CsPb_xSn_{1-x}I_3$ NWs from their absorption spectrum (Figure S9a), and red line is the binomial fitting. (b) Normalized PL spectrum of black phase $CsPb_xSn_{1-x}I_3$ nanowires.

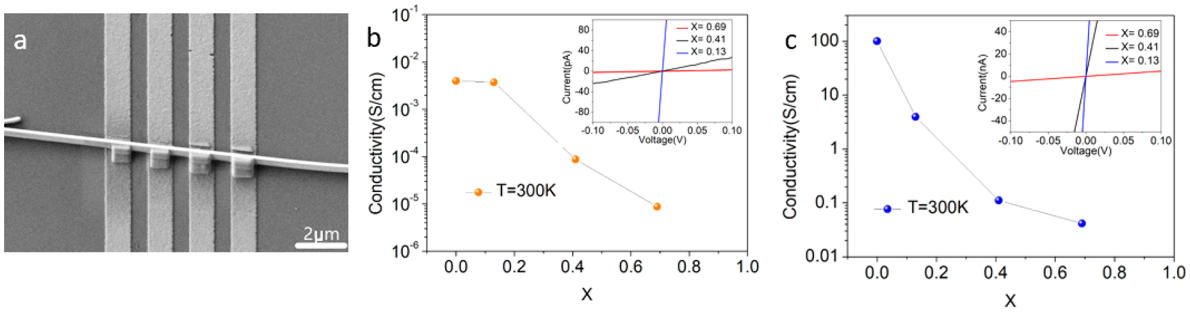

Figure 4. (a) SEM image showing a single NW on the Au electrode after EBID. Conductivity measurement for a yellow (b) and black (c) phase $CsPb_xSn_{1-x}I_3$ NW with three different compositions (x = 0.69, 0.41, and 0.13). Insets show the corresponding IV curve. Conductivity data for yellow and black $CsSnI_3$ comes from refs 24 and 29, respectively.

1.78 eV, which also show band bowing with a bowing factor of 0.57 eV (Figure 3a). The PL emission red shifts from 700 to 950 nm as the Sn contents increase in the NWs, which indicates the PL emission tunability in the near-infrared region (Figure 3b).

To measure the electrical conductivity of the $CsPb_xSn_{1-x}I_3$ NW, a single Y phase $CsPb_xSn_{1-x}I_3$ NW and B-γ phase $CsPb_xSn_{1-x}I_3$ NW were transferred onto prepatterned Au bottom electrodes using a micromanipulator. To make better contacts between the electrodes and NWs, we used electron beam induced deposition (EBID) to deposit Pt at the NW/electrode interface (Figure 4a). Based on previous reports, Y phase $CsSnI_3$ is semiconducting with conductivity around 4×10^{-3} S/cm, while Y phase $CsPbI_3$ is almost insulating.[27,31] For Y phase $CsPb_xSn_{1-x}I_3$ NWs, the conductivity can be tuned with the higher percentage of Sn in the NW leading to it becoming more conductive (Figure 4b). Specifically, for the NWs with 69%, 41%, and 13% Pb, their conductivities are 8.69×10^{-6}, 8.71×10^{-5}, and 3.76×10^{-3} S/cm, respectively. For B-γ phase, the conductivity of $CsSnI_3$ shows metallic behavior such that the conductivity goes down when temperature is increased, while the conductivity of $CsPbI_3$ is still quite low, so a trend similar to the Y phase manifests. By alloying lead and tin together, the electrical conductivity can be tuned between the two extremes. The conductivities for the three corresponding B-γ phase alloy compositions are 4.13×10^{-2}, 1.11×10^{-1}, and 3.94 S/cm, respectively (Figure 4c). It is likely that the conductivity tunability originates from the charge carrier concentration change. It is reported that the main charge carriers, holes in B-γ $CsSnI_3$, result from the Sn vacancy.[25] Therefore, in this Pb−Sn alloy materials system, as the Sn percentage goes up, the number of Sn vacancies in unit volume also increases, which leads to a higher charge carrier concentration and an increase in the conductivity. Generally, B-γ phase $CsPb_xSn_{1-x}I_3$ NWs are more conductive than Y phase $CsPb_xSn_{1-x}I_3$ NWs. For the same composition, B-γ phase $CsPb_xSn_{1-x}I_3$ NWs are 3−4 orders of magnitude more conductive than their Y phase counterparts. To understand the electron−hole character of $CsPb_xSn_{1-x}I_3$ NWs, we also used suspended microisland devices to measure the Seebeck coefficient of individual B-γ phase $CsPb_xSn_{1-x}I_3$ NWs (Figure S10), and the positive sign of the Seebeck coefficient indicates that they are hole-dominant semiconductors, similar to B-γ phase $CsSnI_3$.

In summary, we have successfully synthesized $CsPb_xSn_{1-x}I_3$ NWs, systematically studied the composition and structure of single-crystalline $CsPb_xSn_{1-x}I_3$ NWs, and explored their phase transition, optical, and electrical properties. The band gap of the alloy NWs can be tuned from 1.78 to 1.3 eV, making them potential materials for perovskite tandem photovoltaics as well as near-infrared optical devices. The controlled electrical conductivity paves the way for further exploration for transport and thermoelectric applications in halide perovskites.

■ ASSOCIATED CONTENT

Supporting Information

The Supporting Information is available free of charge on the ACS Publications website at DOI: 10.1021/acs.nanolett.8b00603.

Detailed method for nanowires synthesis, structural and composition characterizations, and optical measurements (PDF)

DOI: 10.1021/acs.nanolett.8b00603
Nano Lett. 2018, 18, 3538−3542

AUTHOR INFORMATION

Corresponding Author

*E-mail: p_yang@berkeley.edu.

ORCID

Teng Lei: 0000-0003-0356-1076

Peidong Yang: 0000-0003-4799-1684

Author Contributions

T.L. and P.Y. designed the experiments. T.L. performed the synthesis of the sample, TEM experiments, XRD experiments, transport measurements, and data analysis. M.L. and D.L. contributed to PL measurement experiments. Q.K. and W.L. contributed to the conductivity measurements. M.L., Q.K., V.W., Y.Y., and L.D. contributed to data analysis. T.L. and P.Y. wrote the manuscript. P.Y. supervised the research project. All authors contributed to the discussions.

Notes

The authors declare no competing financial interest.

ACKNOWLEDGMENTS

This work was supported by the U.S. Department of Energy, Office of Science, Office of Basic Energy Sciences, Materials Sciences and Engineering Division, under Contract DE-AC02-05-CH11231 within the Physical Chemistry of Inorganic Nanostructures Program (KC3103). TEM Work at the NCEM, Molecular Foundry was supported by the Office of Science, Office of Basic Energy Science, of the U.S. Department of Energy under Contract DE-AC02-05CH11231. T.L., M.L., and Q.K. thank Suzhou Industrial Park for the fellowship support. D.L. thanks the Camille and Henry Dreyfus Foundation for funding, Award EP-14-151. We would like to thank Karen Bustillo for the help on TEM measurements.

REFERENCES

(1) Repins, I.; Contreras, M. A.; Egaas, B.; DeHart, C.; Scharf, J.; Perkins, C. L.; To, B.; Noufi, R. *Prog. Photovoltaics* **2008**, *16* (3), 235−239.

(2) Contreras, M. A.; Egaas, B.; Ramanathan, K.; Hiltner, J.; Swartzlander, A.; Hasoon, F.; Noufi, R. *Prog. Photovoltaics* **1999**, *7* (4), 311−316.

(3) Jeon, N. J.; Noh, J. H.; Yang, W. S.; Kim, Y. C.; Ryu, S.; Seo, J.; Seok, S. I. *Nature* **2015**, *517* (7535), 476−480.

(4) Eperon, G. E.; Leijtens, T.; Bush, K. A.; Prasanna, R.; Green, T.; Wang, J. T.-W.; McMeekin, D. P.; Volonakis, G.; Milot, R. L.; May, R. *Science* **2016**, *354* (6314), 861−865.

(5) Kondow, M.; Uomi, K.; Niwa, A.; Kitatani, T.; Watahiki, S.; Yazawa, Y. *Jpn. J. Appl. Phys.* **1996**, *35* (2S), 1273.

(6) Nakamura, S.; Senoh, M.; Nagahama, S.-i.; Iwasa, N.; Yamada, T.; Matsushita, T.; Kiyoku, H.; Sugimoto, Y. *Jpn. J. Appl. Phys.* **1996**, *35* (1B), L74.

(7) Iyer, S. S.; Patton, G. L.; Stork, J. M.; Meyerson, B. S.; Harame, D. L. *IEEE Trans. Electron Devices* **1989**, *36* (10), 2043−2064.

(8) Ning, C.-Z.; Dou, L.; Yang, P. *Nat. Rev. Mater.* **2017**, *2* (12), 17070.

(9) Ye, H. Y.; Liao, W. Q.; Hu, C. L.; Zhang, Y.; You, Y. M.; Mao, J. G.; Li, P. F.; Xiong, R. G. *Adv. Mater.* **2016**, *28* (13), 2579−2586.

(10) Hafez, W.; Lai, J.-W.; Feng, M. *IEEE Electron Device Lett.* **2003**, *24* (7), 436−438.

(11) Lee, M. M.; Teuscher, J.; Miyasaka, T.; Murakami, T. N.; Snaith, H. J. *Science* **2012**, *338* (6107), 643−647.

(12) Zhou, H.; Chen, Q.; Li, G.; Luo, S.; Song, T.-b.; Duan, H.-S.; Hong, Z.; You, J.; Liu, Y.; Yang, Y. *Science* **2014**, *345* (6196), 542−546.

(13) Correa-Baena, J.-P.; Saliba, M.; Buonassisi, T.; Grätzel, M.; Abate, A.; Tress, W.; Hagfeldt, A. *Science* **2017**, *358* (6364), 739−744.

(14) Yang, W. S.; Park, B.-W.; Jung, E. H.; Jeon, N. J.; Kim, Y. C.; Lee, D. U.; Shin, S. S.; Seo, J.; Kim, E. K.; Noh, J. H. *Science* **2017**, *356* (6345), 1376−1379.

(15) Fu, Y.; Meng, F.; Rowley, M. B.; Thompson, B. J.; Shearer, M. J.; Ma, D.; Hamers, R. J.; Wright, J. C.; Jin, S. *J. Am. Chem. Soc.* **2015**, *137* (17), 5810−5818.

(16) Tan, Z.-K.; Moghaddam, R. S.; Lai, M. L.; Docampo, P.; Higler, R.; Deschler, F.; Price, M.; Sadhanala, A.; Pazos, L. M.; Credgington, D. *Nat. Nanotechnol.* **2014**, *9* (9), 687−692.

(17) Zhu, H.; Fu, Y.; Meng, F.; Wu, X.; Gong, Z.; Ding, Q.; Gustafsson, M. V.; Trinh, M. T.; Jin, S.; Zhu, X. *Nat. Mater.* **2015**, *14* (6), 636−642.

(18) Eaton, S. W.; Lai, M.; Gibson, N. A.; Wong, A. B.; Dou, L.; Ma, J.; Wang, L.-W.; Leone, S. R.; Yang, P. *Proc. Natl. Acad. Sci. U. S. A.* **2016**, *113* (8), 1993−1998.

(19) Fu, Y.; Zhu, H.; Stoumpos, C. C.; Ding, Q.; Wang, J.; Kanatzidis, M. G.; Zhu, X.; Jin, S. *ACS Nano* **2016**, *10* (8), 7963−7972.

(20) Dou, L.; Yang, Y. M.; You, J.; Hong, Z.; Chang, W.-H.; Li, G.; Yang, Y. *Nat. Commun.* **2014**, *5*, 5404.

(21) Ramasamy, P.; Lim, D.-H.; Kim, B.; Lee, S.-H.; Lee, M.-S.; Lee, J.-S. *Chem. Commun.* **2016**, *52* (10), 2067−2070.

(22) Jeon, N. J.; Noh, J. H.; Kim, Y. C.; Yang, W. S.; Ryu, S.; Seok, S. I. *Nat. Mater.* **2014**, *13* (9), 897−903.

(23) Swarnkar, A.; Marshall, A. R.; Sanehira, E. M.; Chernomordik, B. D.; Moore, D. T.; Christians, J. A.; Chakrabarti, T.; Luther, J. M. *Science* **2016**, *354* (6308), 92−95.

(24) Chung, I.; Lee, B.; He, J.; Chang, R. P.; Kanatzidis, M. G. *Nature* **2012**, *485* (7399), 486−489.

(25) Chung, I.; Song, J.-H.; Im, J.; Androulakis, J.; Malliakas, C. D.; Li, H.; Freeman, A. J.; Kenney, J. T.; Kanatzidis, M. G. *J. Am. Chem. Soc.* **2012**, *134* (20), 8579−8587.

(26) Lee, W.; Li, H.; Wong, A. B.; Zhang, D.; Lai, M.; Yu, Y.; Kong, Q.; Lin, E.; Urban, J. J.; Grossman, J. C. *Proc. Natl. Acad. Sci. U. S. A.* **2017**, *114*, 8693.

(27) Lai, M.; Kong, Q.; Bischak, C. G.; Yu, Y.; Dou, L.; Eaton, S. W.; Ginsberg, N. S.; Yang, P. *Nano Res.* **2017**, *10* (4), 1107−1114.

(28) Zhang, D.; Yang, Y.; Bekenstein, Y.; Yu, Y.; Gibson, N. A.; Wong, A. B.; Eaton, S. W.; Kornienko, N.; Kong, Q.; Lai, M. *J. Am. Chem. Soc.* **2016**, *138* (23), 7236−7239.

(29) Bernard, J. E.; Zunger, A. *Phys. Rev. B: Condens. Matter Mater. Phys.* **1986**, *34* (8), 5992.

(30) Zhang, D.; Eaton, S. W.; Yu, Y.; Dou, L.; Yang, P. *J. Am. Chem. Soc.* **2015**, *137* (29), 9230−9233.

(31) Yamada, K.; Matsui, T.; Tsuritani, T.; Okuda, T.; Ichiba, S. *Z. Naturforsch., A: Phys. Sci.* **1990**, *45*, 307−312.

DOI: 10.1021/acs.nanolett.8b00603
Nano Lett. 2018, 18, 3538−3542